Structural and electrochemical characterizations of P2 and new O3-NaxMn1-yFeyO2 phases prepared by auto-combustion synthesis for Na-ion batteries

Benoît Mortemard de Boisse, Dany Carlier-Larregaray, Marie Guignard, Claude Delmas

Structural and Electrochemical Characterizations of P2 and New O3-$Na_xMn_{1-y}Fe_yO_2$ Phases Prepared by Auto-Combustion Synthesis for Na-Ion Batteries

B. Mortemard de Boisse,[a,b] D. Carlier,[a,b,z] M. Guignard,[a,b] and C. Delmas[a,b]

[a]*CNRS, Université de Bordeaux, ICMCB, 33608 Pessac Cedex, France*
[b]*CNRS, IPB-ENSCBP, ICMCB, 33608 Pessac Cedex, France*

Abstract: Using auto-combustion synthesis route followed by a 1000°C heat-treatment, we succeeded to prepare four $Na_x(Mn,Fe)O_2$ phases: P2-$Na_{0.67}Mn_{2/3}Fe_{1/3}O_2$, P2-$Na_{0.71}Mn_{1/2}Fe_{1/2}O_2$, and new Na-deficient O3-$Na_{0.82}Mn_{1/3}Fe_{2/3}O_2$ and O3-$Na_{\sim 0.8}Mn_{1/2}Fe_{1/2}O_2$ phases. We studied their structures by X-ray Diffraction and their electrochemical properties as positive electrode in Na-cells that were reversibly charged and discharged in the 1.5 and 3.8 V range vs. Na^+/Na, leading to discharge capacities between 135 and 155 $mAh.g^{-1}$. The shapes of the cycling curves are discussed together with the stacking of the phases and the redox processes involved in the Na intercalation/deintercalation reaction. In some cases the Fe(IV) state is clearly reached.

Layered oxides with Na_xMO_2 formula (M = transition metal), were studied in the 80's for their sodium intercalation (deintercalation) properties, then for next 20 years all the researches were focused on lithium batteries that exhibit the high energy density required for portable devices. In the perspective of the development at very large scale of renewable energy systems, which require stationary batteries, the prevailing parameters are the lifetime, the price and the material availability. From these points of view, sodium based batteries are reinvestigated for several years. In the case of layered oxides only the fully intercalated O3-$LiMO_2$ type structure can be obtained by solid state chemistry at high temperature, while in the case of homologous sodium system several Na_xMO_2 polytypes (P3, P2, O3)[1] can be obtained by high temperature solid state chemistry due to the weakness on the Na-O bond vs. the Li-O one and the tendency of sodium to stabilize the high oxidation states of transition element. As far as applications are expected, the choice of abundant (cheap) elements has to be considered. Iron and manganese being good candidates for this point of view, we focused our interest recently on the $Na_x(Co,Mn)O_2$ and $Na_x(Mn,Fe)O_2$ systems. The structure of the phases and the oxidation states of M cations were characterized in P2-$Na_{2/3}Co_{2/3}Mn_{1/3}O_2$ and in P'3-$Na_{2/3}Mn_{1-y}Fe_yO_2$ (y = 0, 1/3, 2/3) phases.[2,3] Preliminary electrochemical properties were also reported in Na or Li cells. In literature also, several studies were reported on Mn and/or Fe based sodium layered oxides as Na_xMnO_2,[4–13] Na_xFeO_2,[14–16] $Na_x(Ni,Mn)O_2$,[17–19] $Na_x(Ni,Fe,Mn)O_2$,[20] $Na_x(Co,Ni,Mn)O_2$[21] and very recently on $Na_x(Mn,Fe)O_2$.[22,23]

In alkali element deficient Na_xMO_2 phases the charge compensation occurs through oxidation of the trivalent M^{3+} cation to the M^{4+} one. Therefore, the $Na_xM^{3+}{}_xM^{4+}{}_{1-x}O_2$ general charge distribution is expected like in the P2-$Na_{2/3}Co_{2/3}Mn_{1/3}O_2$ system, we recently published.[2] In the $Na_x(Mn,Fe)O_2$ materials obtained by high temperature chemistry, Fe^{3+} and Mn^{4+} ions are expected. Nevertheless, depending on the overall composition, on the synthesis temperature and on the partial oxygen pressure, Mn^{3+} ions can also be stabilized. Moreover, the strong stabilization of Mn^{4+} in oxidizing medium (O_2) can lead, in some cases, to the formation of manganese vacancies for charge compensation as in $Na_{2/3}MnO_2$.[24,25] All these points show that a very special attention must be taken during the material synthesis to the Na:Mn:Fe ratios and to the experimental conditions (temperature, partial oxygen pressure and thermal treatment duration). Moreover, high-spin Mn^{3+} and Fe^{4+} being Jahn-Teller cations, interesting structural and physical properties can occur either in battery deep charge (Fe^{4+}) or discharge (Mn^{3+}).

In this paper, we report the synthesis by auto-combustion of some $Na_xMn_{1-y}Fe_yO_2$, ($0.5 < x < 1$), y = 1/3, 1/2, 2/3 phases, their characterization through X-Ray Diffraction (XRD) and their electrochemical behavior in Na cells.

[z]E-mail: carlier@icmcb-bordeaux.cnrs.fr

Experimental

Auto-combustion synthesis (or self-propagating high temperature synthesis) is characterized by the high temperature quickly reached during the combustion process, typically above 1000 K,[26] which results in the obtention of a homogenous, small-sized precursor or poorly crystallized phase.[27] Even if the classical solid-state route allowed us to prepare some of the phases as also reported,[22,23] the combustion synthesis route allowed the preparation of pure phases for the four materials that we considered. We therefore focused only on these materials in this study.

The experimental procedure used to prepare the P2/O3-$Na_xMn_{1-y}Fe_yO_2$ phases was the following: manganese, iron and sodium nitrates (Alfa Aesar, $Mn(NO_3)_2.4H_2O$ (97% purity), $Fe(NO_3)_3.9H_2O$ (98%) and $NaNO_3$ (99%) respectively) were dissolved in water. The initial stoichiometries used were: (x = 0.77; y = 1/3) and (x = 0.67; y = 1/2) for the P2 phases and (x = 0.81, y = 1/2) and (x = 0.77; y = 2/3) for the O3 phases. Moreover, a 10 wt% excess for $NaNO_3$ was added to take into account the high volatility of sodium. Please note that the sodium content and the Fe/Mn ratio are the key parameters for the preparation of the P2 or O3 phases. After dissolution, glycin was added, representing one eighth of the total nitrate amount (mol.). The solution was then placed into a ceramic bowl on a sand bath heated at 480°C. Once the combustion was complete, the product was ground and heated into a tubular furnace in an alumina boat, first at 700°C for 20 h under air to decompose any remaining traces of nitrates and then at 1000°C for 5 h under O_2 using a +5°C/min heating ramp. The samples were then quenched down to room temperature and stored into an Ar filled glove box. The purity of the various phases was checked using a Philips PW1820 X-Ray Diffractrometer (Cu $k\alpha_{1,2}$) and airtight sample holders. Structural refinements and pattern matching were performed on the XRD patterns recorded in the (10–110°) 2θ range, using the FullProf Suite.[28]

Scanning Electron Microscopy (SEM) micrographs were taken using a Hitachi S-4500 (V = 3.0 kV). The samples were previously gold coated to enhance their electronic conductivity under the electron beam.

The initial raw material composition and Mn:Fe ratios were confirmed by Inductively Coupled Plasma Absorption Emission Spectroscopy (ICP-AES) on a Varian 720ES Apparatus from 10 mg of powder dissolved into boiling HCl/HNO_3 (33/67). The Na composition was then roughly determined based on the Na/(Mn+Fe) ratio, and then determined by the Rietveld refinement of the XRD patterns.

Electrochemical studies were carried out using Na//$NaPF_6$ in Propylene Carbonate (1 M)//$Na_xMn_{1-y}Fe_yO_2$ cells in homemade Swagelok battery-type assembled in an Ar-filled glove box. The positive electrode consisted in a mixture of the active material/Carbon Black/PolyTetraFluoroEthylene in an 88/10/2 mass ratio. The electrolyte was obtained by dissolution of $NaPF_6$ (Alpha Aesar 99+%) in Propylene Carbonate (Sigma-Aldrich anhydrous 99%) to reach a final

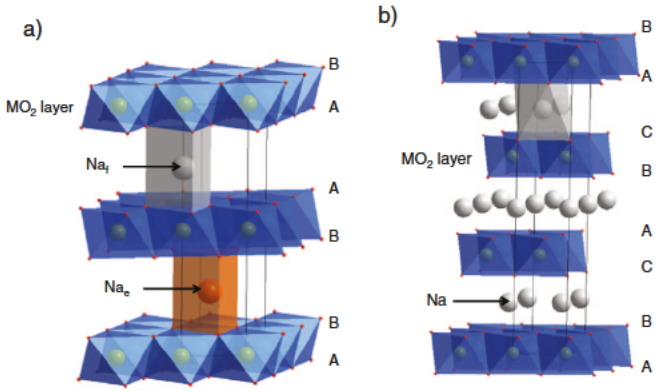

Figure 1. Representation of the P2-type (S.G.: $P6_3/mmc$ (a)) and the O3-type (S.G.: R-3m (b)) structures of the Na_xMO_2 phases. The Na_fO_6 site and Na_eO_6 prisms are respectively sharing faces or edges with the MO_6 octahedra in the P2 phase. In the O3 type the NaO_6 octahedra share only edges with the MO_6 ones.

concentration of 1 mol.l^{-1}. The cells were then tested using a Biologic VMP3 in galvanostatic mode between 1.5 and 3.8 V vs. Na^+/Na redox couple at the C/100 rate (1 mole of Na^+ per formula unit (dis)charged in 100 h). The electrodes were separated by three layers of Whatman glass fiber sheet.

Results and Discussion

Structural characterization.— The study of the $Na_xMn_{1-y}Fe_yO_2$, ($0.5 < x < 1$), $y = 1/3, 1/2, 2/3$ systems prepared at 1000°C shows the existence of several layered phases with P2 or O3 oxygen stackings. These materials crystallize in the hexagonal systems ($P6_3/mmc$ space group) or in the rhombohedral system (R-3m space group), respectively. The schematic view of the structures is given in Fig. 1. In this structural designation the letter P or O indicates the environment of the alkali ion (trigonal prismatic or octahedral) while the Figure 2 or 3 gives the number of MO_2 slabs within the hexagonal cell.[1]

The experimental and calculated XRD patterns of the various synthetized phases are given in Fig. 2 and the corresponding structural parameters are given in Table I. The Atomic Displacement Parameters (ADP or B_{iso}) were fixed to reasonable values (1.0; 0.5; 0.5 and 0.8 Å^2 for sodium, manganese, iron and oxygen respectively). Note that our attempts to refine these values lead to divergence of the refinements. Whereas the $Na_{2/3}Mn_{2/3}Fe_{1/3}O_2$ and $Na_{0.82}Mn_{1/3}Fe_{2/3}O_2$ phases exhibit respectively P2- and O3-type structures, the $Na_xMn_{1/2}Fe_{1/2}O_2$ phases exhibit both stackings depending on the overall final Na content (x): P2 for $x \sim 0.7$ and O3 for $x \sim 0.8$. The XRD patterns show that in all case the samples are well crystallized and pure, except for "$Na_{0.8}Mn_{1/2}Fe_{1/2}O_2$" that contains a small amount of a O'3 type phase, (the prime symbol denoting a monoclinic distortion of the cell: C2/m space group). In this case both phases exhibit very close interslab spaces (Table I). For the 3 first phases the sodium amount deduced from the Rietveld refinement is in good agreement with the

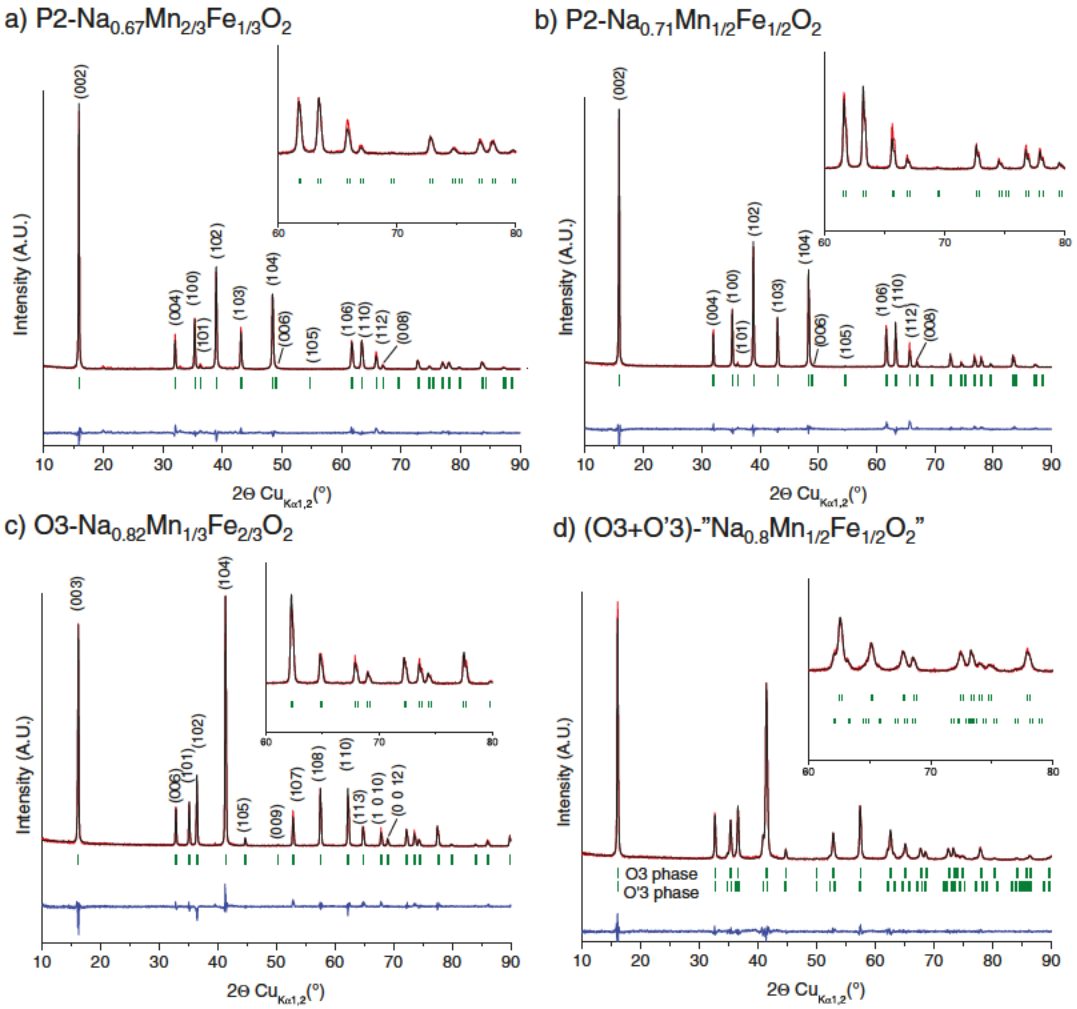

Figure 2. Observed and calculated XRD patterns for (a) P2-$Na_{0.67}Mn_{2/3}Fe_{1/3}O_2$, (b) P2-$Na_{0.71}Mn_{1/2}Fe_{1/2}O_2$, (c) O3-$Na_{0.82}Mn_{1/3}Fe_{2/3}O_2$ and (d) the O3+O'3-"$Na_{0.8}Mn_{1/2}Fe_{1/2}O_2$" mixture: (red) observed; (black) calculated; (blue) lower trace: difference plot; bar: Bragg reflections.

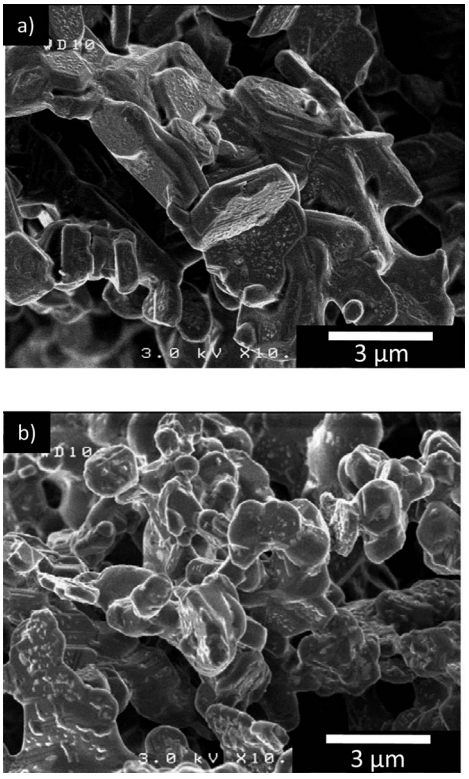

Figure 3. SEM micrographs for (a) P2-$Na_{0.71}Mn_{1/2}Fe_{1/2}O_2$ and (b) O3-$Na_{0.82}Mn_{1/3}Fe_{2/3}O_2$.

results obtained by ICP. In the case of "$Na_{0.8}Mn_{1/2}Fe_{1/2}O_2$", a Rietveld refinement of the Na amount in each phase, O3 and O'3 could not be performed and only the average Na amount based on the ICP measurements is provided.

In our experimental conditions Fe^{3+}, Mn^{4+} and Mn^{3+} ions are expected to be present in the materials. The Mn^{4+}/Mn^{3+} ratio depends on the sodium ion stoichiometry but also of the eventual presence on manganese vacancies in the slab as it was reported for Na_xMnO_{2+y} ($0.05 < y < 0.25$), that can be rewrite as $Na_{2x/(2+y)}Mn_{2/(2+y)}\square_{y/(2+y)}O_2$.[24] This phenomenon has been considered in the Rietveld refinements, nevertheless the amount of transition metal vacancies detected (1–2%) is too small to be considered at this point of the study. From these data, the ideal chemical formulas indicating the amount of the different cations were determined and given in Table I. In agreement with the ideal chemical formula, the MO_2 slab thickness (S) and the *a*-cell parameter (corresponding to $d_{M\text{-}M}$ in-plane distance), are following the relative content of large Fe^{3+} and Mn^{3+} ions ($r = 0.645$ Å) and smaller Mn^{4+} ions ($r = 0.53$ Å). The smaller values for S and *a* are obtained for the P2-$Na_{2/3}Mn_{2/3}Fe_{1/3}O_2$ phase (Table I) in agreement with the larger amount of Mn^{4+} ions. As expected from the various stackings, a larger NaO_2 interslab thickness (IS) is observed for the P2 cells with Na in trigonal prismatic sites than for the O3 one with Na in octahedral sites.

For the $Na_{0.8}Mn_{1/2}Fe_{1/2}O_2$ composition, the monoclinic distortion observed for the O'3 phase could be due to a cooperative Jahn-Teller distortion of the $Mn(III)O_6$ octahedra, and should therefore correspond to a phase with a slightly higher Mn^{3+} content than the O3 one (i.e. slightly higher Na content). Calculation of the b/a ratio of the monoclinic cell give an idea of the magnitude of the distortion: $b/a = 1.77$ for the O'3-$Na_xMn_{1/3}Fe_{2/3}O_2$ that is slightly larger than the ideal ratio for a hexagonal O3 cell described with a mono-

Table I. Cell parameters, sodium sites occupation, oxygen position and profile parameters deduced from the Rietveld refinement data for P2-$Na_{0.67}Mn_{2/3}Fe_{1/3}O_2$, P2-$Na_{0.71}Mn_{1/2}Fe_{1/2}O_2$ and O3-$Na_{0.82}Mn_{1/3}Fe_{2/3}O_2$. For the O3+O'3-$Na_{0.8}Mn_{1/2}Fe_{1/2}O_2$ mixture, only the cell and profile parameters are reported. Standard deviations have been multiplied by the Scorr number to correct from local correlations.[33] The March-Dolasse function was used to describe the preferential orientation of the particles. The Na position in the O3 type cells is the 3b position of the R-3m space group and the Na_e and Na_f positions in the P2 type cells are respectively 2d and 2b positions of the $P6_3/mmc$ space group. Conventional reliability factors of refinements are given.

		P2-$Na_xMn_{2/3}Fe_{1/3}O_2$	P2-$Na_xMn_{1/2}Fe_{1/2}O_2$	O3-$Na_xMn_{1/3}Fe_{2/3}O_2$	(O3+O'3)-$Na_xMn_{1/2}Fe_{1/2}O_2$	
					O3	O'3
Space Group		$P6_3/mmc$	$P6_3/mmc$	R-3m	R-3m	C2/m
Cell parameters	a (Å)	2.9325(3)	2.9390(2)	2.9810(1)	2.9661(2)	5.206(1)
	b (Å)					2.938(1)
	c (Å)	11.175(2)	11.182(1)	16.321(1)	16.402(2)	5.754(1)
	β (°)					108.00(1)
Refined coordinates	z (Oxygen)	0.092(1) 4f position	0.096(1) 4f position	0.267(1) 6c position		
Profile parameters (Pseudo-Voigt function)	u	0.16(3)	0.21(1)	0.06(1)	0.16(6)	0.09(4)
	v	−0.03(2)	0.001(1)	−0.05(1)	0.07(7)	−0.10(3)
	w	0.025(3)	0.019(3)	0.047(3)	0.01(2)	0.066(5)
	Shape (η)	0.60(3)	0.65(3)	0.38(3)	0.96(4)	0.41(2)
preferred orientation ⊥ to c axis		1.05(9)	1.06(9)	1.04(7)		
R_B (%)		7.37	10.1	9.82		
R_{wp} (%)		19.2	19.0	22.9	16.0	
Scorr number		3.00	3.09	2.53	2.03	
NaO_2 Interslab (IS) thickness (Å)		3.531(2)	3.444(2)	3.275(2)		
MO_2 Slab (S) thickness (Å)		2.056(2)	2.150(2)	2.165(2)		
Interslab distance (Å)		5.588(2)	5.591(2)	5.440(2)	5.467(2)	5.472(1)
Occupation of Na site	Na_f (P2)	0.235(6)	0.232(7)			
	Na_e(P2)	0.438(6)	0.473(7)			
	Na (O3)			0.82(1)		
	Total Na	0.67	0.71	0.82	0.80 (from ICP measurement)	
Theoritical amount of	Mn(III)	1/3	0.21	0.15	0.3	
	Mn(IV)	1/3	0.29	0.18	0.2	
	Fe(III)	1/3	1/2	2/3	1/2	

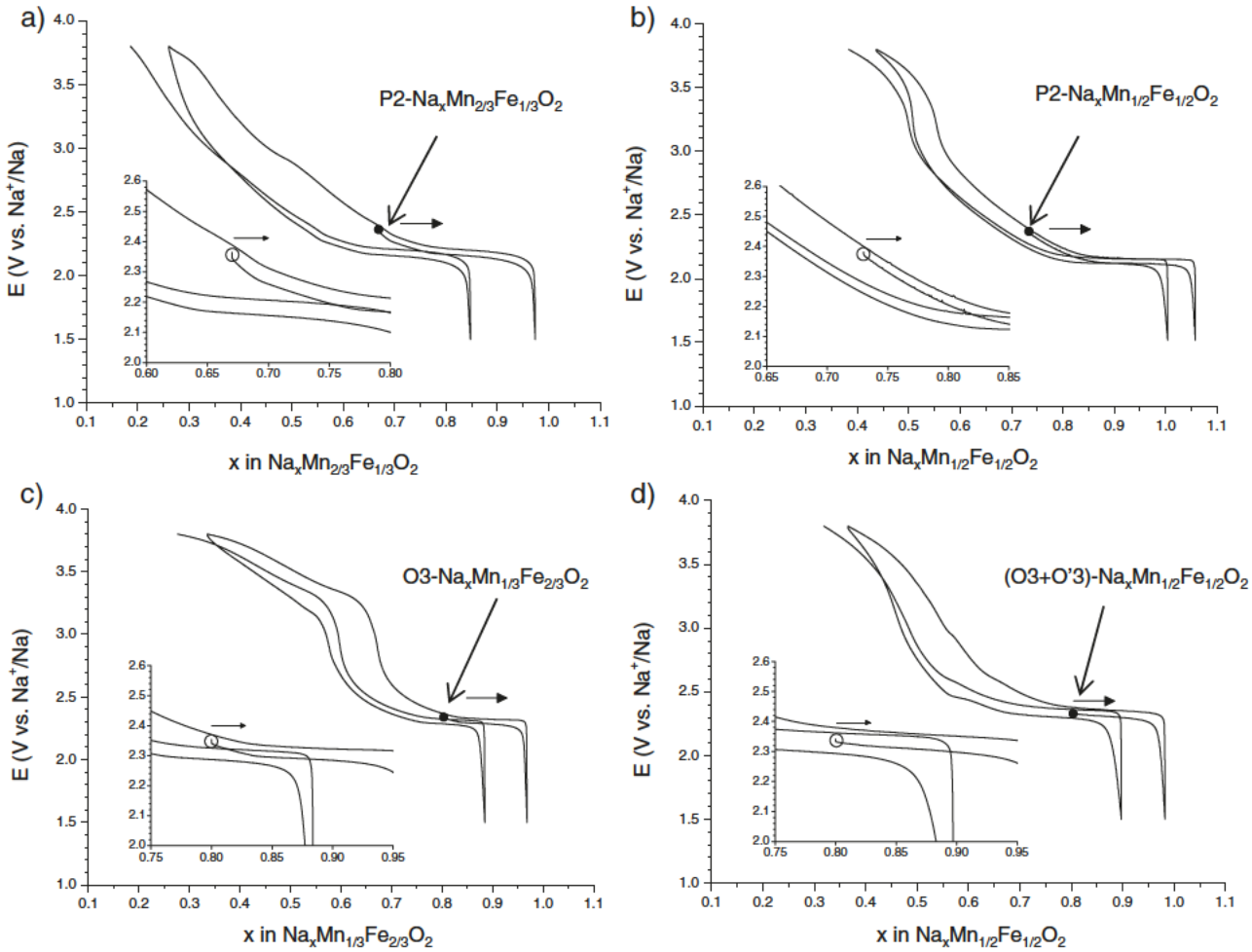

Figure 4. Galvanostatic cycling curves of the Na//Na$_x$(Mn,Fe)O$_2$ cells obtained with a C/100 cycling rate, starting by a discharge: (a) P2-Na$_x$Mn$_{2/3}$Fe$_{1/3}$O$_2$; (b) P2-Na$_x$Mn$_{1/2}$Fe$_{1/2}$O$_2$; (c) O3-Na$_x$Mn$_{1/3}$Fe$_{2/3}$O$_2$ and (d) O3-Na$_x$Mn$_{1/2}$Fe$_{1/2}$O$_2$. A magnification of each curve around the starting point is shown in the insets.

clinic cell (b/a = 1.73 ($\sqrt{3}$)), but still much lower than the distortion observed in O'3-NaMnO$_2$ (b/a = 1.94[29]) for which all manganese ions are high spin-Mn^{3+}. The presence of a cooperative Jahn-Teller distortion is surprising as the phase also contains a large amount of non Jahn-Teller Fe^{3+} and/or Mn^{4+} ions. Further investigation of the phase diagram around this composition and of the local transition metal ions environments will be required. The other phases, that do not exhibit a macroscopic distortion of the cell, might also exhibit some local distortion of the Mn(III)O$_6$ octahedra.

The particles morphologies are shown in Fig. 3 through the SEM micrographs of the P2-Na$_{0.71}$Mn$_{1/2}$Fe$_{1/2}$O$_2$ and the O3-Na$_{0.82}$Mn$_{1/3}$Fe$_{2/3}$O$_2$ phases. These samples are representative of the two different kinds of phases. The P2-type phases exhibit well-shaped particles with 3.4 µm average diameter and 200 nm thickness. The O3-type phases show round-shaped particles of 3 µm average size. The small imperfections on the surface of both phases are due to air exposition during the gold sputtering and increased both in number and size with the exposure time. We believe that NaOH /Na$_2$CO$_3$ are formed on the surface as the sodium is rejected from the structure, allowing the average Mn oxidation state to increase. All phases present agglomerated particles with larger sizes than the ones reported by Yabuuchi et al.[23] (500 nm mean size). This is certainly related to the higher synthesis temperature that we used.

Electrochemical properties in Na cells.— All the Na$_x$Mn$_{1-y}$Fe$_y$O$_2$, (0.5 < x < 1), y = 1/3, 1/2, 2/3 phases were tested as positive electrode in Na batteries. Fig. 4 shows the evolution of the potential of the cells as a function of the Na content (x) cycled between 1.5 and 3.8 V vs. Na$^+$/Na. Identical behaviors were observed, starting by a charge or by a discharge (only the curves starting by a discharge are shown here). One can notice that in the case of the P2-Na$_x$Mn$_{1/2}$Fe$_{1/2}$O$_2$ (Fig. 4b), a fully-discharged state with sodium content higher than 1 is obtained. This can be a consequence either of a slightly wrong estimation of the Na content by the Rietveld refinement of the XRD patterns or a consequence of the presence of some transition metal vacancies as mentioned above. For every single phase, the charge and discharge curves look quite similar, indicating a good reversibility of the Na intercalation/deintercalation process (Fig. 4). We note that a partial degradation of the electrolyte occurs above around 3.5 V vs. Na$^+$/Na. In order to discuss the cell capacities, we therefore considered only the discharge curves.

Fig. 5a compares the evolution of the discharge capacities along with the cycle number. The initial discharge starting from our Na-deficient phases are not shown in Fig. 5a. One can notice that the P2 phases exhibit a higher discharge capacity than the O3 ones. By comparison to the literature, the discharge capacity we obtained for the P2-Na$_x$Mn$_{1/2}$Fe$_{1/2}$O$_2$ is lower than the one observed by Yabuuchi et al. (~145 mAh.g^{-1} vs. ~190 mAh.g^{-1}).[23] This difference can be explained by various factors: i) the higher voltage limitation used in their study: 4.3 V vs. Na$^+$/Na (we, unfortunately, could not reach similar voltage because of large electrolyte degradation); ii) the different electrode design; and iii) the different size of the crystallites: around 3 µm diameter in our case, which is much larger than the 500 nm mean size reported in Ref. 23. Taking all these factors into account, it is thus

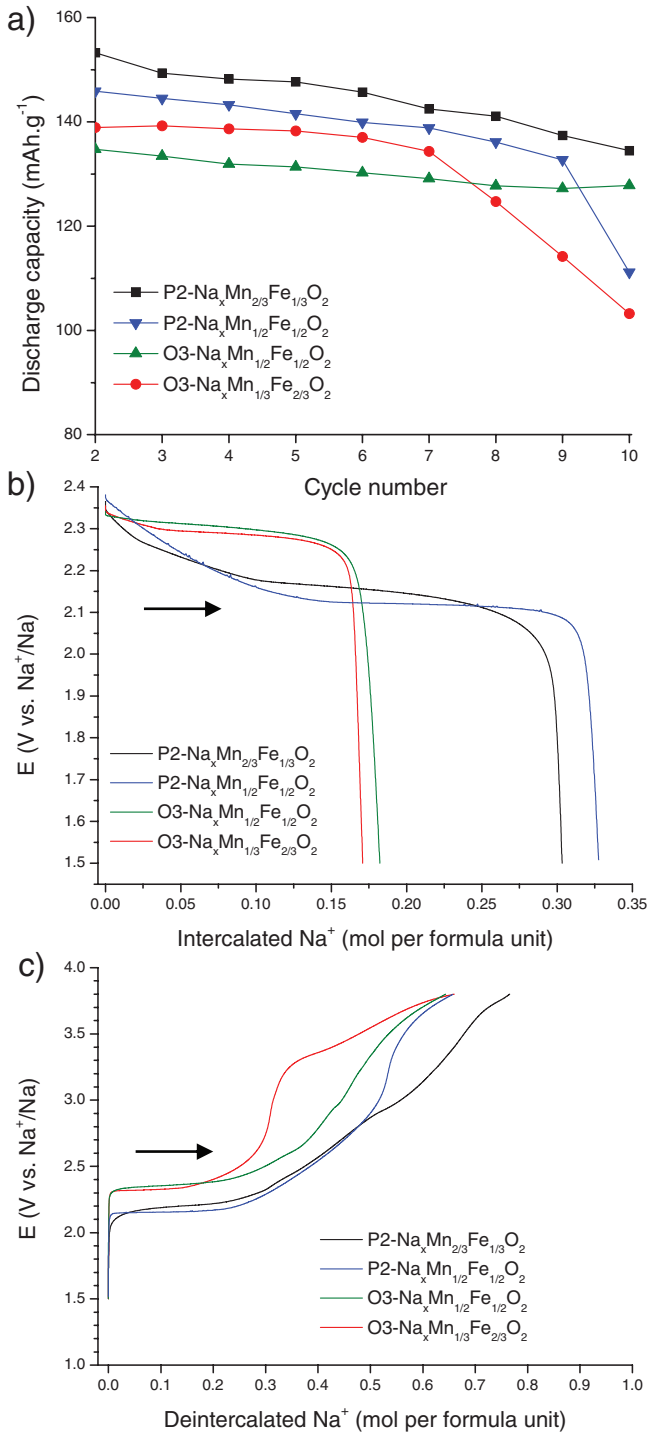

Figure 5. (a) Evolution of the discharge capacities of the different Na//$Na_x(Mn,Fe)O_2$ cells; (b) comparison between the first discharge of the four materials; (c) comparison between the first charge following the initial discharge for the four materials plotted as a function of the capacity.

surprising that the discharge capacities of our O3-$Na_xMn_{1/2}Fe_{1/2}O_2$ and O3-$Na_xMn_{1/3}Fe_{2/3}O_2$ phases are higher than the one reported in Refs. 22 and 23 (~135 mAh.g^{-1} vs. ~110 mAh.g^{-1} respectively for O3-$Na_xMn_{1/2}Fe_{1/2}O_2$ and ~140 mAh.g^{-1} vs. 90 mAh.g^{-1} for O3-$Na_xMn_{1/3}Fe_{2/3}O_2$). It could come from a different amount of transition metal vacancies in the slab thus stabilizing Mn^{4+} as different preparation conditions were used (we prepared O3 phases with initial Na amount lower than one (vs. one in Refs. 22 and 23) and a 1000°C final heat-treatment under O_2 atmosphere (vs. 700°C in air in Ref. 23)). However, it could also come from the use of higher cutoff voltages that can lead for Iron based materials to some irreversible Fe migration in the alkaline layer during charging as suggested for O3-$NaFeO_2$.[16] More characterizations are needed to distinct the effects of these different factors in those materials (P2 vs. O3 and O3 vs. literature).

Fig. 5b compares the first discharge curves recorded for the four materials. As expected from the estimated Na contents in our P2 and O3 phases, more Na can be intercalated in the P2 phases that are more Na-deficient (around + 0.32 and + 0.18 mol of Na /formula unit respectively for the P2 phases and O3 phases). Nevertheless, this clearly confirms that the synthetized O3 phases exhibit an initial Na content lower than one.

Fig. 5c shows the cycling curves recorded during the first charge (following the initial discharge). All phases exhibit a plateau at the beginning of the charge, characteristic of the existence of a biphasic domain. The plateau is slightly higher in voltage for the O3 phases (+0.2 V) vs. the P2 ones, indicating that a higher energy is required to remove the Na^+ ion for the inter-layer space in the O3 oxygen stacking, and partially explains why the discharge capacities of the O3 phases are lower than the ones observed for the P2 phases. Similar differences in voltage were obtained for the Na_xVO_2 phases.[30–32] The presence of a voltage plateau for the O3-$Na_xMn_{1/2}Fe_{1/2}O_2$ system indicates that it is electrochemically different from the O3-$NaMn_{1/2}Fe_{1/2}O_2$ phase reported by Yabuuchi et al.,[23] that only exhibits a continuous increase of the potential as the sodium content decreases, in agreement with different discharge capacities obtained in the two cases. Note that the starting point of the galvanostatic curve for the $Na_xMn_{1/2}Fe_{1/2}O_2$ compound (Fig. 4d) is located on the plateau, in good agreement with the observation of two phases O3(majority) + O'3(minority) in the XRD pattern. The intercalation of Na in our system should therefore lead to a fully intercalated O'3-$NaMn_{1/2}Fe_{1/2}O_2$ phase and not to an O3 one as reported to be obtained by solid state reaction by Yabuuchi et al.[23] Note that every attempt to synthesize a pure Na-deficient O3-$Na_xMn_{1/2}Fe_{1/2}O_2$ phase (therefore using a slightly lower sodium content than x = 0.8) led to P2+O3 mixtures or pure P2 phases.

During the first charge (following the first discharge), the Na^+ ions deintercalation should be associated first to the Mn(III)→ Mn(IV) oxidation process followed by the Fe(III)→Fe(IV) one. Depending on the Mn/Fe initial stoichiometry, the second process can be achieved or not in our experiments. The iron richest phases studied here, i.e, O3-$Na_xMn_{1/3}Fe_{2/3}O_2$, actually exhibits a sudden voltage increase for x ~ 2/3 (~1/3 Na deintercalated) that is a good agreement with the change of active redox couples (Mn ions are present only in the +IV state in O3-$Na_{2/3}Mn^{(IV)}{}_{1/3}Fe^{(III)}{}_{2/3}O_2$). Similar voltage jump is also observed, for the P2-$Na_xMn_{1/2}Fe_{1/2}O_2$ phase as expected around x ~ 0.5, but is less pronounced for the O3-$Na_xMn_{1/2}Fe_{1/2}O_2$ system. In the case of the P2-$Na_xMn_{2/3}Fe_{1/3}O_2$ system, because of low iron content, the oxidation of iron is hardly reached in our cycling conditions.

Conclusion

Using auto-combustion synthesis route followed by a 1000°C heat-treatment we succeeded to prepare two P2-$Na_x(Mn,Fe)O_2$ (x ~ 0.70) phases and two new O3-$Na_x(Mn,Fe)O_2$ ones that exhibit a Na-deficiency (x ~ 0.80). Between 1.5 and 3.8 V vs. Na^+/Na, the O3 phases exhibit discharge capacities (around 135–140 mAh.g^{-1}) only slightly below the one of the P2 ones (145–150 mAh.g^{-1}). We believe that their performances could be highly improved by reducing the electrolyte decomposition issue. The O3 phases are definitely new as their behavior is different form the one reported in literature for O3-$Na(Mn,Fe)O_2$[22,23] phases. These differences could come from the different preparation conditions, as we prepared O3 phases with initial Na amount lower than one (vs. one in Refs. 22 and 23) and a 1000°C final heat-treatment under O_2 atmosphere (vs. 700°C in air in Ref. 23). Actually these systems (O3 but also P2) have to be considered in a more complex diagram than the one just implying different Na:Mn:Fe ratios, since they could present transition metal vacancies in the slab thus stabilizing more Mn^{4+} ions as expected form the ideal

formula. Therefore, various initial Na:Mn:Fe ratios and experimental conditions (temperature, partial oxygen pressure and thermal treatment duration) can lead to different $Na_x(Mn,Fe)O_{2+y}$ phases, that can be rewrite as $Na_{2x/(2+y)}(Mn,Fe)_{2/(2+y)}\square_{y/(2+y)}O_2$. Further experiments will be required to better characterize these systems.

Acknowledgments

This work benefited from a grant from Agence Nationale de la Recherche (Blanc Inter II, SIMI 8) n° 2011-IS08-001-01. Région Aquitaine and CNRS are also acknowledged for B.M scholarship. C. Denage, M. Arnault, P. Dagault are acknowledged for experimental support.

References

1. C. Delmas, J. J. Braconnier, C. Fouassier, and P. Hagenmuller, *Solid State Ionics*, **3/4**, 165 (1981).
2. D. Carlier, J. H. Cheng, R. Berthelot, M. Guignard, M. Yoncheva, R. Stoyanova, B. J. Hwang, and C. Delmas, *Dalton Trans.*, **40**, 9306 (2011).
3. M. Yoncheva, R. Stoyanova, E. Zhecheva, E. Kuzmanova, M. Sendova-Vassileva, D. Nihtianova, D. Carlier, M. Guignard, and C. Delmas, *J. Mater. Chem.*, **22**, 23418 (2012).
4. C. Fouassier, C. Delmas, and P. Hagenmuller, *Mater. Res. Bull.*, **10**, 443 (1975).
5. A. Mendiboure, C. delmas, and P. Hagenmuller, *J. Solid State Chem.*, **57**, 323 (1985).
6. J. M. Tarascon, D. G. Guyomard, and B. Wilkens, *Solid State Ionics*, **57**, 113 (1992).
7. A. Caballero, L. Hernan, J. Morales, L. Sanchez, J. Santos Pena, and M. A. G. Aranda, *J. Mater Chem.*, **12**, 1142 (2002).
8. M. M. Doeff, T. J. Richardson, and K. T. Hwang, *J. Power Sources*, **135**, 240 (2004).
9. F. Sauvage, L. Laffont, J. M. Tarascon, and E. Baudrin, *Inorg. Chem.*, **46**, 3289 (2007).
10. J. F. Whitacre, A. Trevar, and S. Sharma, *Electrochem. Comm.*, **12**, 463 (2010).
11. X. Ma, H. Chen, and G. Ceder, *J. Electrochem. Soc.*, **158**(12), A1307 (2011).
12. E. Hosono, T. Saito, J. Hoshino, M. Okubo, Y. Saito, D. Nishio-Hamane, T. Kudo, and H. Zhou, *J. Power Sources*, **217**, 43 (2012).
13. H. Kim, D. J. Kim, D-H. Seo, M. S. Yeom, K. Kang, D. K. Kim, and Y. Jung, *Chem. Mater.*, **24**(6), 1205 (2012).
14. K. M. Abraham and D. M. Pasquariello, *J. Electrochem. Soc.*, **137**, 1189 (1990).
15. Y. Takeda, K. Nakahara, M. Nishijima, N. Imanishi, O. Yamamoto, M. Takano, and R. Kanno, *Mater. Res. Bull.*, **29**(6), 659 (1994).
16. N. Yabuuchi, H. Yoshida, and S. Komaba, *Electrochemistry*, **80**(10), 716 (2012).
17. Z. Lu and J. R. Dahn, *J. Electrochem. Soc.*, **148**(11), A1225 (2001).
18. S. Komaba, T. Nakayama, A. Ogata, T. Shimizu, C. Takei, S. Takada, A. Hokura, and I. Nakai, *ECS Transactions*, **16**(42), 43 (2009).
19. S. Komaba, N. Yabuuchi, T. Nakayama, A. Ogata, T. Ishikawa, and I. Nakai, *Inorg. Chem.*, **51**, 6211 (2012).
20. D. Kim, E. Lee, M. Slater, W. Lu, S. Rood, and C. S. Johnson, *Electrochem. Comm.*, **18**, 66 (2012).
21. M. Sathiya, K. Hemalatha, K. Ramesha, J. M. Tarascon, and A. S. Prakash, *Chem. Mater.*, **24**(10), 1846 (2012).
22. N. Yabuuchi, J. Iwatate, M. Kajiyama, Y. Yamamoto, S. Hitomi, R. Okuyama, and S. Komaba, *220th ECS Meeting*, Abstract #649 (2011).
23. N. Yabuuchi, M. Kajiyama, J. Iwatate, H. Nishikawa, S. Hitomi, R. Okuyama, R. Usui, Y. Yamada, and S. Komaba, *Nature Mater.*, **11**, 512 (2012).
24. C. Fouassier, C. Delmas, and P. Hagenmuller, *Mater. Res. Bull.*, **10**, 443 (1975).
25. R. Stoyanova, D. Carlier, M. Sendova-Vassileva, M. Yoncheva, E. Zhecheva, D. Nihtianova, and C. Delmas, *J. Solid State Chem.*, **183**, 1372 (2010).
26. J. J. Moore and H. J. Feng, *Prog. Mater. Sci.*, **39**, 243 (1995).
27. F. Mauvy, J.-M. Bassat, E. Boehm, P. Dordor, and J.-P. Loup, *Solid State Ionics*, **158**, 395 (2003).
28. J. Rodriguez-Carvajal, Laboratoire Léon Brillouin, http://www-llb.cea.fr/fullweb/powder.htm.
29. F. Capitaine, P. Gravereau, and C. Delmas, *Solid State Ionics*, **89**, 197 (1996).
30. D. Hamani, M. Ati, J. M. Tarascon, and P. Rozier, *Electrochem. Comm.*, **13**, 938 (2011).
31. C. Didier, M. Guignard, C. Denage, O. Szajwaj, S. Ito, I. Saadoune, J. Darriet, and C. Delmas, *Electrochem. Solid-State Lett.*, **14**(5), A75 (2011).
32. M. Guignard, C. Didier, J. Darriet, P. Bordet, E. Elkaïm, and C. Delmas, *Nature Mater.*, (2012).
33. T. Roisnel and J. Rodriguez-Carvajal, *Mater. Sci. Forum*, **378-381**, 118 (2001).